Chapter 12

QUASI-THREE-DIMENSIONAL BLADE PASSAGE FLOW FIELD ANALYSIS

The aerodynamic design and analysis of multistage axial-flow compressors is usually based on empirical cascade performance models as described in Chapters 6 through 11. Although that approach is sufficient for most applications, designers occasionally require the support offered by more fundamental internal flow analyses. When a specific application requires operating a blade row at conditions more extreme than justified by experience, supplemental analysis can greatly increase the designer's confidence or perhaps prevent a poor decision. In the case of industrial axial-flow compressors, this usually relates to the blade row inlet Mach number level. The industrial compressor designer usually has a number of discrete geometrical scales or frame sizes available. If a specific application slightly exceeds the upper limit of flow capacity for a frame size, the designer must either accept somewhat higher Mach number levels or choose a larger frame size with a substantial increase in cost. Alternatively, transonic blade sections such as double-circular-arc blades might be considered. Usually that also involves increased cost and may be unattractive with respect to structural integrity. Even when the application is well within the normal flow capacity limits of a frame size, an unusual working fluid or a required rotation speed can result in Mach number levels beyond the designer's experience. In those cases, designers need a more fundamental internal flow analysis to better evaluate probable impact of the higher Mach number levels.

Chapter 5 presented several useful techniques for the analysis of the internal flow on stream surfaces within blade passages. Those blade-to-blade flow analyses can provide the desired detailed evaluation, but all of them require that the stream surface geometry and stream sheet thickness be specified in some fashion. An approximate analysis can be conducted using the stream sheet geometry before and after the blade row from the meridional through-flow analysis of Chapter 7, while assuming a linear variation between those stations. That is certainly the fastest and simplest approach and often may be considered sufficient.

Alternatively, a more accurate analysis can be conducted using the quasi-three-dimensional flow analysis technique mentioned in Chapters 3 and 5. That is a very efficient analysis technique that provides a reasonable approximation to the three-dimensional flow field through a blade row. Originally suggested by Wu

(1952), this technique relies on solving for the two-dimensional flow on the blade-to-blade stream surfaces and on the hub-to-shroud stream surface, with interaction between them until they are consistent with each other. This chapter describes a quasi-three-dimensional flow analysis suitable for that purpose. This analysis was originally developed for centrifugal compressors (Aungier, 2000), where it plays an essential role in the aerodynamic design of impellers. It was subsequently extended to treat arbitrary three-dimensional blade geometry for additional flexibility in centrifugal impeller design. That extension made it possible to use the analysis directly for axial-flow compressor blade rows.

The only special extension added for axial-flow compressors is provision for automatic generation of detailed blade geometry for all of the standard blade profiles discussed in Chapter 4. This permits complete blade specification in terms of the radial variation of the basic blade section parameters (e.g., θ, γ, c and t_b/c). The same capability is incorporated into the various blade-to-blade flow analyses of Chapter 5 for a single blade section. Hence it is relatively simple to provide the capability to automatically set up input files for either a simple blade-to-blade analysis on a single stream surface or a quasi-three-dimensional flow analysis for a blade passage directly from a completed meridional through-flow analysis. In the author's design and analysis system, both the performance analysis of Chapter 9 and the design system of Chapter 11 contain that provision. When a more detailed analysis is needed, it can be obtained in a few minutes with very little additional effort.

NOMENCLATURE

B^* = stream surface repositioning damping factor
b = stream sheet thickness
C = absolute velocity
D = stream surface curvature damping factor
E = entrainment function
f = blade force
g = $2\pi r\cos\beta'/Z$
H = total enthalpy
H_1 = meridional shape factor = δ_1^*/θ_{11}
H_2 = boundary layer tangential shape factor = δ_2^*/θ_{22}
h = static enthalpy
I = rothalpy
K_B = blade blockage factor
M = Mach number
m = meridional coordinate
$\dot{m}$ = mass flow rate
n = normal coordinate
P = pressure
q = inlet dynamic head
r = radius
s = entropy
T = temperature

t_b = blade thickness
W = velocity relative to the blade row
y = distance along quasi-normal
Z = number of blades
z = axial coordinate
β = flow angle
ΔA = stream sheet area
Δv = increment in v due to blade guidance
δ = boundary layer thickness
δ_c = blade clearance
δ_1^* = boundary layer meridional displacement thickness
δ_2^* = boundary layer tangential displacement thickness
ε = angle between quasi-normal and true normal
η = dimensionless tangential coordinate
θ = tangential coordinate and streamwise momentum thickness
θ_{11} = meridional momentum thickness
θ_{22} = tangential momentum thickness
κ = camberline angle with meridional direction
κ_m = stream surface curvature
λ = quasi-normal angle (Fig. 12-3)
v = blade force defect thickness
ρ = fluid density
ϕ = stream surface angle with the axial direction
ω = rotation speed, radians/sec.

Subscripts

h = parameter at the hub contour
m = meridional component
s = parameter at the shroud contour
θ = tangential component

Superscripts

$'$ = parameter in rotating coordinates
$\bar{}$ = mass-averaged value

12.1 QUASI-THREE-DIMENSIONAL FLOW

Figure 12-1 shows a meridional plane view of a blade row to be analyzed. The annular passage is divided into a series of stream sheets, separated by stream surfaces. All stream sheets are defined to contain equal mass flow. For simplicity, it is assumed that all stream surfaces are axisymmetric, i.e., stream sheet twisting will be ignored. The meridional coordinate, m, is measured along a stream sheet's mean surface, and the stream sheet thickness is designated as b. If the stream sur-

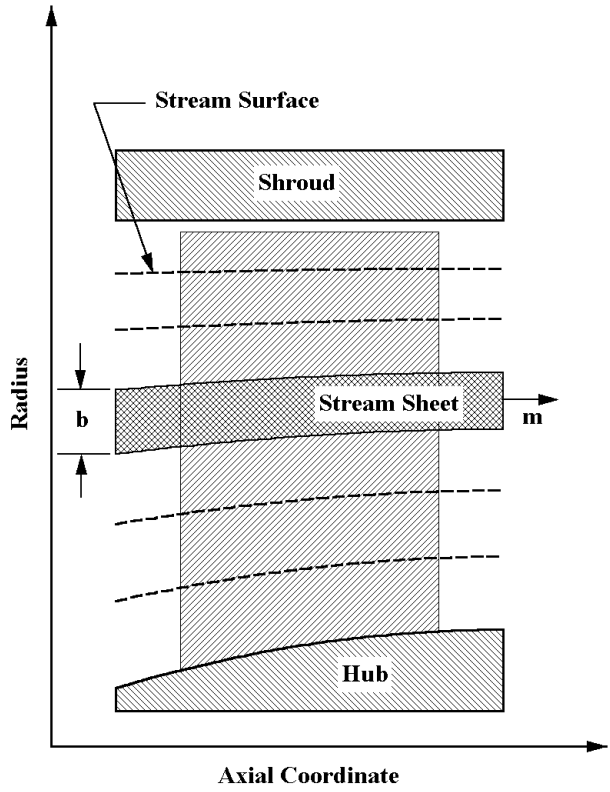

FIGURE 12-1 Hub-to-Shroud Flow Geometry

faces and the distribution of b are known, a complete two-dimensional blade-to-blade flow analysis can be conducted using one of the methods described in Chapter 5. Figure 12-2 shows a typical blade-to-blade surface view to illustrate the solution domain for one of the blade-to-blade flow analyses to be conducted. Since blade-to-blade flow analysis has been covered extensively in Chapter 5, it is only necessary to identify the specific method to be used. The best choice for quasi-three-dimensional flow analysis is the linearized potential flow analysis of Section 5.4, including the extension to transonic flow. That method offers exceptional computation speed and reliability as well as excellent prediction accuracy for compressor blade rows. To be sure, the two-dimensional blade-to-blade flow analyses offer somewhat better accuracy. But it is still possible to take advantage of those more general analyses when needed. The linearized method is quite adequate to provide support to the hub-to-shroud flow analysis, such that accurate stream surface locations and stream sheet thicknesses are obtained. Once the quasi-three-dimensional flow analysis is complete, all input data needed for the two-dimensional blade-to-blade flow analyses are available. It is quite simple to make provision to generate input files for those more exact methods for any or all stream surfaces—that is a

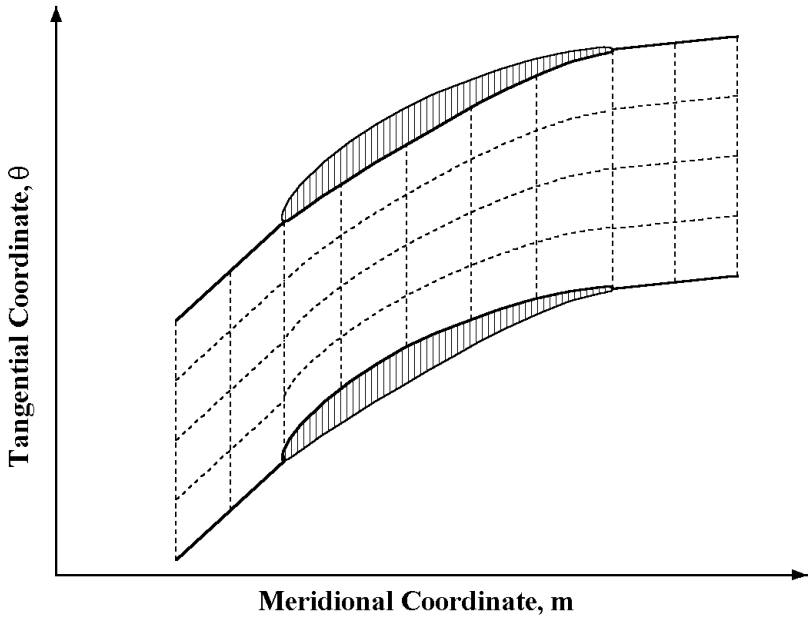

FIGURE 12-2 Blade-to-Blade Flow Geometry

more efficient approach than incorporation of the more exact methods directly into the quasi-three-dimensional flow analysis. Indeed, it is not uncommon for a complete quasi-three-dimensional flow analysis to require significantly less computer time than a blade-to-blade flow analysis for the same problem on a single stream sheet by the two-dimensional blade-to-blade flow analyses.

The hub-to-shroud flow analysis usually predicts the average meridional through flow in the passage. Alternatively, the meridional flow field on a mean hub-to-shroud stream surface is sometimes predicted. The prediction of the average through flow will be used in this chapter, since it is more consistent with the assumption of axisymmetric blade-to-blade stream surfaces. The hub-to-shroud flow analysis is similar to the meridional through-flow analysis of Chapter 7, except that the tangential momentum equation is no longer satisfied by conservation of angular momentum. Indeed, the distribution of angular momentum through the blade row must be obtained from the blade-to-blade flow analyses for all stream surfaces.

12.2 HUB-TO-SHROUD FLOW GOVERNING EQUATIONS

The hub-to-shroud flow analysis is conducted using the quasi-normal coordinate system introduced in Chapter 7 for the meridional through-flow analysis. The basic nomenclature and construction of that coordinate system developed in Chapter 7 are summarized in the following equations and in Fig. 12-3.

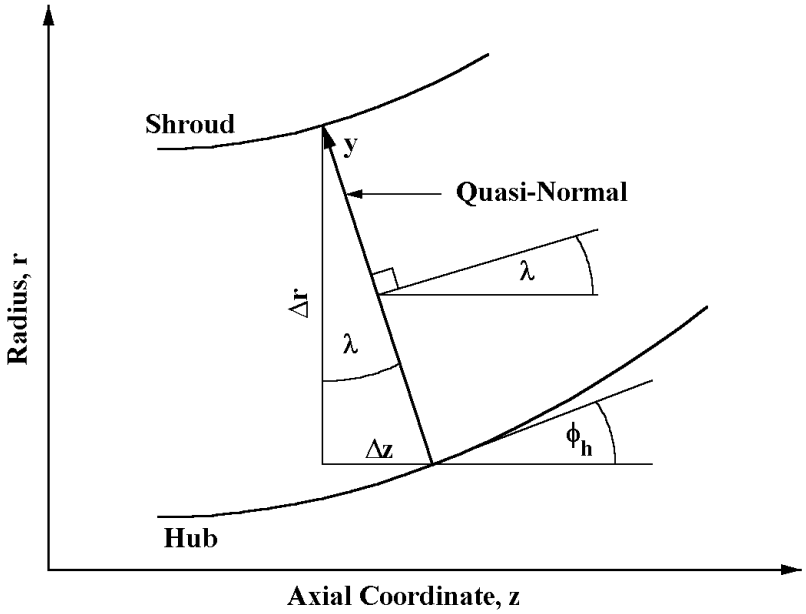

FIGURE 12-3 Quasi-Normal Geometry

$$\tan\lambda = \frac{\Delta z}{\Delta r} = \frac{z_h - z_s}{r_s - r_h} \tag{12-1}$$

$$\sin\phi = \frac{\partial r}{\partial m} \tag{12-2}$$

$$\varepsilon = \phi - \lambda \tag{12-3}$$

$$\frac{\partial}{\partial n} = \frac{1}{\cos\varepsilon}\left[\frac{\partial}{\partial y} - \sin\varepsilon\frac{\partial}{\partial m}\right] \tag{12-4}$$

$$\kappa_m = -\frac{\partial\phi}{\partial m} \tag{12-5}$$

The relevant equations for adiabatic inviscid flow are developed in general form in Chapter 3 in a natural coordinate system. For the present application, Eqs. (3-21), (3-25) and (3-30) apply after they are simplified to their time-steady form. It will be convenient to satisfy conservation of mass in integral form rather than using Eq. (3-21). Conservation of mass along a quasi-normal can be expressed in the form

$$\dot{m} = 2\pi\int_0^{y_s} K_B r\rho W_m \cos\varepsilon\, dy \tag{12-6}$$

K_B is the blade blockage factor, which corrects the stream sheet area available for through-flow to account for blade metal blockage. If the angle formed by a tangent to the blade camberline with respect to the meridional direction is denoted by κ, K_B is given by

$$K_B = 1 - t_b Z / (2\pi r \cos\kappa) \tag{12-7}$$

Consistent with the blade-to-blade flow analysis to be used, rothalpy and entropy are assumed to be constant on stream surfaces, but may vary in the direction normal to the stream surfaces. Using Eqs. (3-25) and (3-30), these assumptions can be expressed by

$$\frac{\partial I}{\partial \theta} = \frac{\partial s}{\partial \theta} = 0 \tag{12-8}$$

$$\frac{\partial I}{\partial m} = \frac{\partial s}{\partial m} = 0 \tag{12-9}$$

$$\kappa_m W_m^2 + \frac{W_\theta}{r}\frac{\partial (rW_\theta + \omega r^2)}{\partial n} + W_m \frac{\partial W_m}{\partial n} = \frac{\partial I}{\partial n} - T\frac{\partial s}{\partial n} \tag{12-10}$$

Equation (12-10) can be solved for W_m if W_θ, s and I are known on all stream surfaces. I and s can be supplied through assigned upstream boundary conditions, just as was done for the meridional through-flow analysis in Chapter 7. Equations (12-8) and (12-9) provide values at all other points in the flow field. The distribution of W_θ on the stream surfaces must be obtained from the blade-to-blade flow analysis. Combining Eqs. (3-29) and (12-8),

$$\frac{\partial (rW_\theta + \omega r^2)}{\partial m} = \frac{\partial W_m}{\partial \theta} \tag{12-11}$$

Chapter 5 develops the blade-to-blade flow analysis for axisymmetric stream surfaces. Indeed, Eq. (12-11) is the principal momentum equation used in the blade-to-blade flow analysis. Clearly, a hub-to-shroud flow analysis restricted to axisymmetric stream surfaces can match only a single distribution of W_θ in the meridional plane. The most logical choice is to use a mass-averaged distribution of W_θ obtained from the blade-to-blade flow analyses on the various stream surfaces. In effect, the hub-to-shroud flow analysis will generate an axisymmetric flow field that is consistent with the mass-averaged angular momentum distribution produced by the blade-to-blade flow analyses. Equation (12-11) is basically ignored by this approximate hub-to-shroud analysis for all points within a blade passage. This equation can be satisfied for points upstream and downstream of the blade passage, where the conservation of the mass-averaged angular momentum is required. In this case, Eq. (12-11) can be written as

$$\frac{\partial (rW_\theta + \omega r^2)}{\partial m} = \frac{\partial rC_\theta}{\partial m} = 0 \tag{12-12}$$

Since the linearized blade-to-blade flow analysis of Chapter 5 applies only to points within the blade passage, Eq. (12-12) is required to treat points outside the blade passage. Combining Eqs. (3-1), (12-4), (12-9) and (12-10) yields the normal momentum equation in the quasi-normal coordinate system.

$$\frac{\partial W_m}{\partial y} + \left[\kappa_m \cos\varepsilon - \frac{\sin\varepsilon}{W_m}\frac{\partial W_m}{\partial m}\right] W_m + \frac{W_\theta}{rW_m}\left[\frac{\partial rC_\theta}{\partial y} - \sin\varepsilon \frac{\partial rC_\theta}{\partial m}\right] = \frac{1}{W_m}\left[\frac{\partial I}{\partial y} - T\frac{\partial s}{\partial y}\right] \tag{12-13}$$

For points outside the blade passage where Eq. (12-12) can be applied, it is easily seen that Eq. (12-13) is identical to Eq. (7-12), which is used for the meridional through-flow analysis. For points within the blade passage it is more convenient to express the angular momentum in terms of the relative flow angle, noting that $W_\theta = W_m \tan\beta'$. This yields

$$\left[\kappa_m \cos\varepsilon - \frac{\sin\varepsilon}{W_m \cos^2\beta'}\frac{\partial W_m}{\partial m} + \frac{\tan\beta'}{r}\left(\frac{\partial r\tan\beta'}{\partial y} - \sin\varepsilon\frac{\partial r\tan\beta'}{\partial m}\right)\right] W_m + \frac{1}{\cos^2\beta'}\frac{\partial W_m}{\partial y} + 2\omega\tan\beta'(\cos\lambda - \sin\phi\sin\varepsilon) = \frac{1}{W_m}\left[\frac{\partial I}{\partial y} - T\frac{\partial s}{\partial y}\right] \tag{12-14}$$

For points outside the blade passage where Eq. (12-12) applies, Eq. (12-14) should reduce to the form used in the meridional through-flow analysis of chapter 7, i.e., to Eq. (7-14). Introducing $W_\theta = W_m \tan\beta'$ into Eq. (12-12), it is easily shown that

$$\frac{W_m \tan\beta'}{r}\frac{\partial r\tan\beta'}{\partial m} = -\tan^2\beta'\frac{\partial W_m}{\partial m} - 2\omega\sin\phi\tan\beta' \tag{12-15}$$

Substituting Eq. (12-15) into (12-14) does yield Eq. (7-14) as required. While the two forms are mathematically equivalent, some care is recommended when formulating a numerical analysis. Equations (12-13) and (12-14) are necessary when the angular momentum distribution is supplied externally by the blade-to-blade flow analyses. But outside of the blade passage where Eq. (12-12) is applicable, use of Eqs. (7-12) and (7-14) is likely to result in a more accurate numerical solution.

12.3 NUMERICAL INTEGRATION OF THE GOVERNING EQUATIONS

The mass and momentum conservation equations can be numerically integrated for a specified stream surface geometry and flow angle distribution through the blade passage. The numerical method used is basically identical to the method used in chapter 7. The momentum equation is written in the form

$$\frac{\partial W_m}{\partial y} = f_1(y)W_m + f_2(y) + \frac{f_3(y)}{W_m} \tag{12-16}$$

where f_1, f_2 and f_3 are known functions of y. For quasi-normals within the blade passage,

$$f_1(y) = \cos^2\beta' \left[-\kappa_m \cos\varepsilon - \frac{\tan\beta'}{r}\left(\frac{\partial r \tan\beta'}{\partial y} - \sin\varepsilon \frac{\partial r \tan\beta'}{\partial m} \right) \right] + \frac{\sin\varepsilon}{W_m}\frac{\partial W_m}{\partial m} \tag{12-17}$$

$$f_2(y) = -2\omega\cos\beta' \sin\beta' [\cos\lambda - \sin\phi \sin\varepsilon] \tag{12-18}$$

$$f_3(y) = \cos^2\beta' \left[\frac{\partial I}{\partial y} - T\frac{\partial s}{\partial y} \right] \tag{12-19}$$

For quasi-normals upstream and downstream of the blade passage,

$$f_1(y) = -\kappa_m \cos\varepsilon + \frac{\sin\varepsilon}{W_m}\frac{\partial W_m}{\partial m} \tag{12-20}$$

$$f_2(y) = 0 \tag{12-21}$$

$$f_3(y) = \frac{\partial I}{\partial y} - T\frac{\partial s}{\partial y} - \frac{W_\theta}{r}\frac{\partial (rC_\theta)}{\partial y} \tag{12-22}$$

At the upstream boundary, it is usually more convenient to supply boundary conditions in the stationary frame of reference, in terms of distributions of H, s and either C_θ or β. The first case is easily modeled by substituting C_θ for W_θ and H for I in Eq. (12-22). When the distribution of β is known, Eqs. (7-19) through (7-21), in the stationary frame of reference, yield

$$f_1(y) = \cos^2\beta \left[-\kappa_m \cos\varepsilon - \frac{\tan\beta}{r}\frac{\partial (r\tan\beta)}{\partial y} + \frac{\sin\varepsilon}{W_m}\frac{\partial W_m}{\partial m} \right] \tag{12-23}$$

$$f_2(y) = 0 \tag{12-24}$$

$$f_3(y) = \cos^2\beta \left[\frac{\partial H}{\partial y} - T\frac{\partial s}{\partial y} \right] \tag{12-25}$$

For specified stream surface geometry and flow angle distributions through the blade passage, f_1, f_2 and f_3 will be evaluated at all grid points before integrating the momentum equation. This process is straightforward with the exception of the meridional gradient of W_m in f_1, which depends on the solution. Usual practice is to use values of W_m from the previous iteration to evaluate this gradient. That approach can result in numerical stability problems in cases where W_m is changing rapidly between iterations. Since W_m appears in the denominator, it can also produce singular results when W_m approaches zero. Aungier (2000) suggests a better approach based on simple conservation of mass in all stream

sheets. If the local through-flow area of a stream sheet is designated by ΔA, conservation of mass in the stream sheet requires

$$\Delta \dot{m} = \rho W_m \Delta A \tag{12-26}$$

Then the meridional gradient in f_1 can be replaced by

$$\frac{1}{W_m}\frac{\partial W_m}{\partial m} = -\frac{1}{\rho \Delta A}\frac{\partial \rho \Delta A}{\partial m} \tag{12-27}$$

This expresses the gradient in terms of the stream sheet geometry and gas density. The stream sheet geometry is constant during the process of integrating the mass and momentum conservation equations. It is still necessary to rely on values of gas density from the previous iteration, but density normally does not vary greatly between successive iterations. Since the mass flow rate in all stream sheets is constant, the risk of singular results is also eliminated. Aungier (2000) uses the same approach to remove the singularity in Eq. (12-16) when W_m approaches zero by defining a new function, f_4, as

$$f_4(y) = f_2(y) + f_3(y)\frac{\rho \Delta A}{\Delta \dot{m}} \tag{12-28}$$

Then Eq. (12-16) can be written as

$$\frac{\partial W_m}{\partial y} = f_1(y) W_m + f_4(y) \tag{12-29}$$

The solution of this linear differential equation has already been given in Chapter 7 as

$$W_m(y) = W_m(0)F(y) + F(y)\int_0^y \frac{f_4(y)}{F(y)}dy \tag{12-30}$$

where

$$F(y) = \exp\left[\int_0^y f_1(y)dy\right] \tag{12-31}$$

The meridional velocity on the hub contour, $W_m(0)$, is the constant of integration. It is determined from conservation of mass through Eq. (12-6). Equations (12-29) and (12-6) are solved in an iterative numerical scheme, successively improving the estimate of $W_m(0)$ until mass is conserved and the momentum equation is satisfied. This requires calculation of thermodynamic properties such as ρ, using an appropriate equation of state from Chapter 2. At any point, the relative total enthalpy is given by Eq. (3-13), i.e.,

$$H' = I + \tfrac{1}{2}(r\omega)^2 \tag{12-32}$$

The local static enthalpy is given by

$$h = H' - \tfrac{1}{2}W^2 \tag{12-33}$$

Then static thermodynamic conditions are computed from relative total thermodynamic conditions for the change in enthalpy, $(h - H')$, while holding entropy constant. The entropy and rothalpy on each stream surface is known from the assigned upstream boundary conditions. Similarly, the angular momentum, rC_θ, upstream of the blade on each stream surface is known from the assigned upstream boundary conditions. The angular momentum downstream of the blade on each stream surface is obtained from the solution at the blade trailing edge quasi-normal.

12.4 REPOSITIONING STREAM SURFACES

After integrating the mass and momentum conservation equations, the new flow field data is generally not consistent with the resident stream sheet geometry. The correct stream sheet geometry can be computed by integrating Eq. (12-6) across the passage at each quasi-normal and interpolating for the new stream sheet positions such that all stream sheets contain equal mass flow rates. In practice, fairly sophisticated numerical damping procedures are required to avoid numerical instability problems. This writer uses the numerical damping procedure suggested by Novak (1973). For quasi-normals outside of the blade passages Novak recommends

$$\frac{1}{F} = 1 + \frac{(1 - M_m^2)(\Delta y)^2}{B^*(\Delta m)^2} \tag{12-34}$$

F is the fraction of the distance between the new and old stream sheet positions that will actually be used in repositioning the stream sheets, Δy is the hub-to-shroud quasi-normal length, Δm is the minimum meridional spacing between quasi-normals, M_m is the meridional Mach number and B^* is an empirical constant. For quasi-normals inside the blade passage, Novak suggests

$$\frac{1}{F} = 1 + \frac{(1 - M'^2)(\cos\beta'\Delta y)^2}{B^*(\Delta m)^2} \tag{12-35}$$

This damping procedure has been found to be quite effective as long as M_m and M' are limited to be no greater than 0.9. B^* values used are typically in the range of 8 to 16, but the numerical procedure should adjust B^* automatically based on whether the stream surface position errors are increasing or decreasing on successive iterations.

12.5 THE HUB-TO-SHROUD FLOW ANALYSIS

To start the solution, an initial guess must be supplied for all flow field data used in the hub-to-shroud solution. Since no blade-to-blade flow analysis results are available at this point, the initial guess must include an approximate blade-to-blade flow definition. This writer uses the following procedure to initialize the flow field data:

- Stream surfaces are positioned such that all stream sheets contain the equal through-flow area on each quasi-normal.
- Entropy and rothalpy are computed for all stream surfaces from the upstream boundary conditions.
- The meridional velocity is computed from local conservation of mass assuming the local gas density is equal to the relative total density.
- C_θ upstream of the blade is obtained from conservation of angular momentum, Eq. (12-12), using the upstream boundary conditions. This includes the blade leading edge quasi-normal.
- The blade is assumed to provide perfect guidance to the flow over the last 85% of the blade passage length based on the blade camberline angle, κ.
- C_θ downstream of the blade is obtained from conservation of angular momentum using the value at the trailing edge quasi-normal.
- An "inlet slip" condition is applied over the first 15% of the blade passage length based on the relative flow angle computed at leading edge quasi-normal and the blade camberline angle, κ, i.e.,

$$\tan\beta' = \tan\beta'_{LE} + (\tan\kappa - \tan\beta'_{LE})[(m - m_{LE})/(m_{TE} - m_{LE})/0.15]^2 \quad (12\text{-}36)$$

This initialization procedure is very conservative and is virtually certain to successfully start the analysis. But Eq. (12-36) is a rather crude approximation for the blade-to-blade flow that often results in difficult and slow convergence of the hub-to-shroud flow analysis. Once the first blade-to-blade flow analysis results are obtained, convergence of the hub-to-shroud analysis consistently improves dramatically. A much more efficient overall analysis is obtained by simply not requiring convergence on the first attempt at the hub-to-shroud flow analysis. This writer simply limits the number of iterations on the hub-to-shroud flow governing equations on this first attempt to, say 10-12, while ignoring the convergence requirement. This is sufficient to obtain a reasonable stream sheet pattern to run the first blade-to-blade flow analysis.

The general procedure used for the hub-to-shroud flow analysis is a direct application of the well-known streamline curvature technique. The basic conservation equations are solved at each quasi-normal using the procedures described in Section 12.3. Then the stream surfaces are repositioned as described in Section 12.4. The process is repeated until the stream surface positions and flow field data have converged within an acceptable tolerance. This procedure is adequate for most problems, but Aungier (2000) suggests two simple extensions that can greatly improve the reliability of the analysis to the point that a converged

solution is almost always obtained: First, the hub-to-shroud flow analysis should check for choked flow, and limit the overall mass flow rate to the choke value when it occurs. In the nomenclature of Section 12.3, the flow on any quasi-normal is locally beyond the choke limit when

$$\frac{\partial \dot{m}}{\partial W_m(0)} \leq 0 \tag{12-37}$$

where $\dot{m}$ is the calculated mass flow rate obtained from Eq. (12-6). When this condition is encountered, the solution procedure should determine the mass flow rate for which this gradient term is zero, which is the choke value. The choked flow condition of Eq. (12-37) is not always an indication of true choked flow. Often it is caused by numerical errors during the early iterations. The solution should proceed using the largest acceptable mass flow rate, but not exceeding the specified mass flow rate. In the case of a temporary choke due to numerical error, the mass flow rate will gradually increase to the specified value as the solution converges. This simple procedure avoids the most common cause of solution divergence. Another common cause of solution divergence is numerical errors in the streamline curvature terms. The numerical damping of the stream surface repositioning given in Section 12.4 avoids most of these problems. But that damping procedure is indirect with respect to the curvature terms. This writer also imposes a direct damping procedure that can be expressed as

$$\kappa_m \rightarrow (\kappa_{m_i} + D\kappa_{m_{i-1}}) / (1 + D) \tag{12-38}$$

where the subscripts i and i-1 refer to the iteration number and D is a damping factor. Typically, D = 1 is used, but D is increased if successive iterations show a significant increase in convergence errors.

12.6 COUPLING THE TWO BASIC FLOW ANALYSES

The quasi-three-dimensional flow analysis is obtained by coupling the hub-to-shroud flow analysis described in this chapter with the linearized blade-to-blade flow analysis described in Chapter 5. The hub-to-shroud flow analysis defines the stream sheet geometry and corresponding blade geometry for the blade-to-blade flow analysis. The stream sheet thickness is also required, which is computed from the hub-to-shroud flow data and the specified stream sheet mass flow by simple conservation of mass.

$$b = \Delta \dot{m} / (2\pi r K_B \rho W_m) \tag{12-39}$$

Similarly, when the blade-to-blade flow analysis is completed, the results are mass-averaged across the blade passage to provide the relative flow angle distribution to be used on the next hub-to-shroud flow analysis. Recalling that the

dimensionless tangential coordinate, η, used in the blade-to-blade flow analysis varies from 0 to 1, the data required are given by

$$\overline{W}_m = \frac{\int_0^1 \rho b W_m^2 d\eta}{\int_0^1 \rho b W_m d\eta} \tag{12-40}$$

$$\overline{W}_\theta = \frac{\int_0^1 \rho b W_m W_\theta d\eta}{\int_0^1 \rho b W_m d\eta} \tag{12-41}$$

$$\tan \beta' = \overline{W}_\theta / \overline{W}_m \tag{12-42}$$

In addition to requiring convergence of the two component analyses, a convergence criterion is needed for the overall quasi-three-dimensional flow analysis. This writer requires that all relative flow angles predicted by Eq. (12-42) on successive blade-to-blade flow analyses converge within an acceptable tolerance.

Figure 12-4 shows a basic flow chart for the quasi-three-dimensional flow analysis. The combination of the present hub-to-shroud analysis with the linearized blade-to-blade flow analysis of Chapter 5 provides a very reliable and effi-

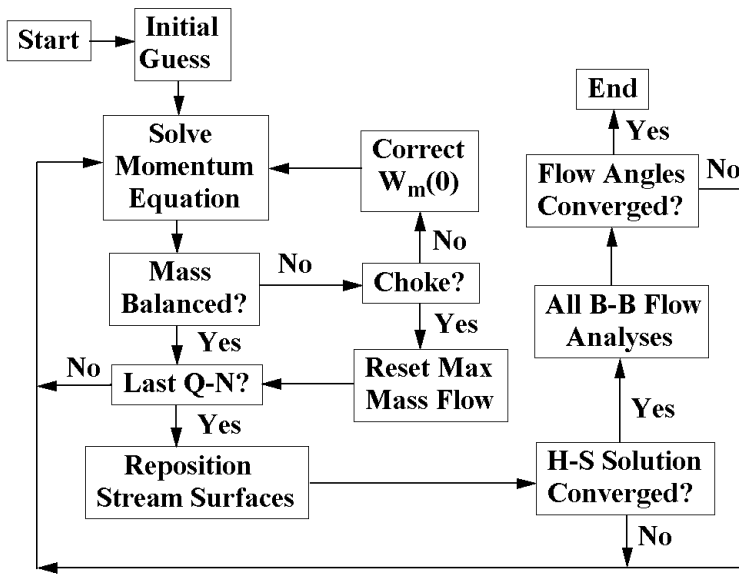

FIGURE 12-4 Flow Chart of the Analysis

cient quasi-three-dimensional flow analysis for a wide range of axial-flow compressor blade passage problems of interest. The major limitation is with regard to Mach number levels, since the blade-to-blade flow analysis cannot account for shock waves. That analysis does have the transonic extension described in Chapter 5, so some supersonic flow is acceptable. The other major restriction follows from the basic assumption of inviscid flow. This is a reasonable assumption as long as the incidence angles are reasonable and flow diffusion is not excessive. Extreme incidence angles or excessive diffusion will result in substantial flow separation, which cannot be modeled by an inviscid flow analysis. To obtain meaningful results, those cases require a more fundamental viscous computational fluid dynamics code.

This analysis requires a very large number of equation-of-state calculations. The pseudo-perfect gas equation of state model described in Chapter 2 can greatly reduce the computational time relative to real gas models, or even ideal gas models with temperature-dependent specific heats. This model is almost always adequate for blade passage flow analyses in compressors. This follows from the fact that some care is normally taken to avoid any risk of operating compressors with liquid present in the flow. Hence the operating conditions are normally safely in the super-heat zone, where gas properties do not show significant variation over the limited range of conditions needed for a flow field analysis. In contrast, turbine applications may involve two-phase flow, or inlet conditions very close to the vapor saturation line. In either case, the pseudo-perfect gas model is usually not adequate for those problems.

Quasi-three-dimensional flow analysis plays a central role in the aerodynamic design of blades for centrifugal compressors, where each blade row is typically a unique design for the specific application (Aungier, 2000). As discussed at the beginning of this chapter, its role for axial-flow compressors is more likely to involve an evaluation of a specific blade row operating under conditions more extreme than justified by experience. To be effective in that role, the analysis must be easily applied as well as fast and reliable. The author's analysis includes the methods described in Chapter 4 to very precisely define the blade geometry for standard axial-flow compressor blade camberlines and profiles to minimize the geometry data required. This, in turn, makes it quite simple to provide the performance analysis of Chapter 9 and the aerodynamic design program of chapter 11 with the capability to export a complete input file for the present analysis. Hence a more detailed evaluation of any blade row analyzed in one of those programs can be accomplished with very little effort.

The performance analysis conducted on the NACA 10-stage compressor in Chapter 9 will be used to illustrate a typical application of this analysis. With reference to Fig. 9-4, the performance analysis for a mass flow rate of 55 at 100% speed predicts that the first stator operates at a supercritical Mach number along the hub contour. Although the performance analysis does not indicate any significant adverse results, the designer might want to evaluate this situation closely. The empirical models for estimating the critical Mach number are certainly quite approximate, and the NACA 65-series blades used are not well suited to operating with significant supersonic flow. To evaluate this situation, a quasi-three-dimensional flow analysis input file for this stator was exported from the performance analysis. After running the quasi-three-dimensional flow analysis, an input file

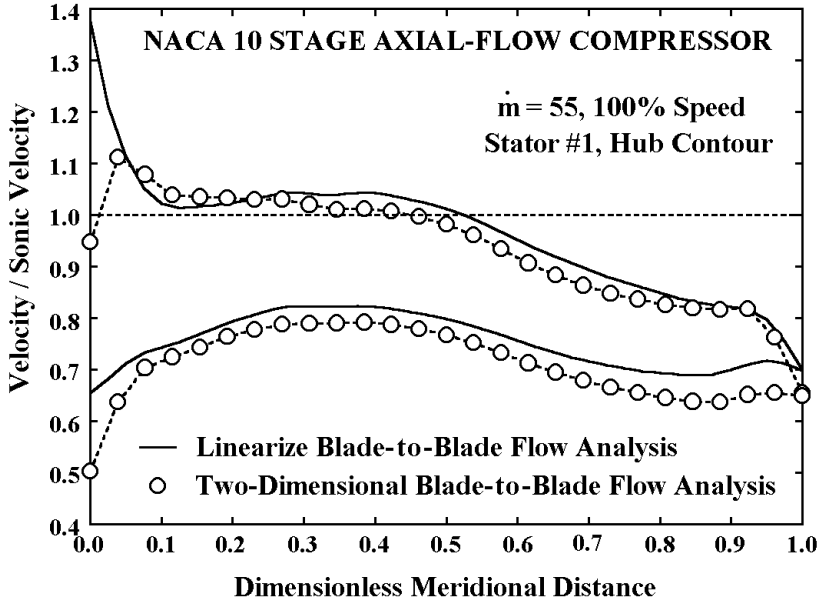

FIGURE 12-5 A Blade Loading Evaluation

for the two-dimensional blade-to-blade flow analysis of Chapter 5, Section 5.3, for the hub surface was exported and processed for a more accurate analysis on this critical stream surface. Figure 12-5 presents the results from these two analyses. It is seen that the stator does operate at a supercritical Mach number. As noted in Chapter 5, blade-loading data close to the leading edge predicted by the linearized blade-to-blade flow analysis should generally be ignored. In that context, the internal flow analyses indicate that the flow is only slightly supersonic and should not pose any significant risk of a performance penalty. The entire process of completing two internal flow analyses to evaluate this situation was accomplished in less than two minutes. That is an important advantage offered by inclusion of efficient inviscid internal flow analysis techniques in a well-formulated aerodynamic design and analysis system. Had a fundamental viscous CFD code been used for this purpose, the evaluation might easily have taken several days. This analysis really encourages designers to evaluate areas of concern, which might otherwise be ignored due to the prohibitive effort required for a more detailed evaluation.

12.7 BOUNDARY LAYER ANALYSIS

Boundary layer analysis provides a useful extension to an inviscid internal flow analysis. It can provide an approximate evaluation of viscous effects with no significant increase in computation time. Chapter 5 describes a two-dimensional

blade surface boundary layer analysis and loss coefficient model that can be incorporated into the quasi-three-dimensional flow field analysis directly. Those models are strictly applicable to just two-dimensional cascade flows. They ignore the secondary flows that are always present in a real cascade. Nevertheless, they do provide a reasonable qualitative evaluation of viscous effects that can provide useful guidance to the designer. Unlike the case of blade surface boundary layers, there is little merit in considering two-dimensional models for the highly three-dimensional end-wall boundary layers. Nor is there much merit today in considering use of inviscid flow analysis coupled with three-dimensional boundary layer analysis models. That approach would involve computation times and complexity comparable to a viscous CFD code, but would offer less generality and accuracy. With the many excellent commercially available viscous CFD codes available today, there is no reason to consider more approximate methods unless they offer substantial advantages in terms of computation speed and reliability. Aungier (2000) uses an end-wall boundary layer analysis that is an early version of the analysis described in Chapter 8. That end-wall boundary layer analysis has since been upgraded to include some of the newer developments described in Chapter 8. This type of axisymmetric, three-dimensional boundary layer analysis is about the only method that can provide meaningful results and offer the computation speed and reliability required. This approximation is known to yield excellent results in vaneless passages [Aungier, 1988(b) and Davis, 1976]. Within the blade passages, the boundary layers are certainly not axisymmetric. There the model seeks to predict the gap-averaged boundary layer behavior (Horlock, 1970) as discussed in Chapter 3.

The description of the end-wall boundary layer analysis provided in Chapter 8 is directly applicable here with two very specific exceptions: In Chapter 8, all meridional computing stations lie outside of the blade passages, so when blade rows are encountered, the meridional integration step is always across the blade row. In the present application, there will be many meridional computing stations within the blade passage. The process of numerical integration remains the same, but here the boundary layer equations are integrated over many spatial steps within the blade passage instead of a single spatial step across it. That, in turn, requires revision of the blade force defect model for it to be applicable within the blade passage. Aungier (2000) suggests the following blade force defect thickness model:

$$\nu = K\theta_{11} \tag{12-43}$$

Based on experimental data from Koch and Smith (1976) and Hunter and Cumpsty (1982), values of K in the range of 0.7 to 1 were recommended. Since those sets of experimental data are from axial-flow compressor tests, it is not too surprising that this simple model yields reasonable results for axial-flow compressor applications. However, since Aungier (2000) was published, a number of centrifugal compressor applications have been encountered where the results did not appear realistic. The weakness in the model has been most evident during analysis of the boundary layer within a blade passage where both the blades and the wall are rotating. As the angle ϕ becomes large, the centrifugal forces in the boundary layer also become large, tending to reduce θ_{11} and, therefore, ν. Under some conditions,

this can produce nearly uniform meridional velocity profiles and highly distorted tangential velocity profiles. It is evident that such highly skewed boundary layer profiles are not reasonable within the blade passages, where blades will tend to guide the flow toward a collateral boundary layer condition. The analysis of Aungier (2000) does not recognize that extreme skewing of the boundary layer flow profiles will be constrained by the flow guidance imposed by the blades.

These observed weaknesses in the method described in Aungier (2000) have recently been significantly improved by adapting the blade force defect model of Chapter 8 to the present application. Figure 12-6 shows the same experimental data as Fig. 8-5 and the simplified empirical correlation used in the present application. Since the present analysis is intended for single blade passage analyses, the larger values of displacement thickness observed in the rear stages of multistage compressors will not be encountered. With little likelihood of approaching the maximum postulated in Fig. 8-5, the simpler linear empirical correlation is a reasonable approximation, which eliminates the staggered spacing term in the correlation. Hence the basic blade force defect thickness of Eq. (8-44) is replaced by

$$v_0 = 0.4\delta_1^* + \delta_c / 2 \tag{12-44}$$

It can be seen that Eq. (12-44) is similar to Eq. (12-43), but is based on the displacement thickness rather than the momentum thickness and includes the influence of the blade clearance. Following the approach used in Chapter 8, the

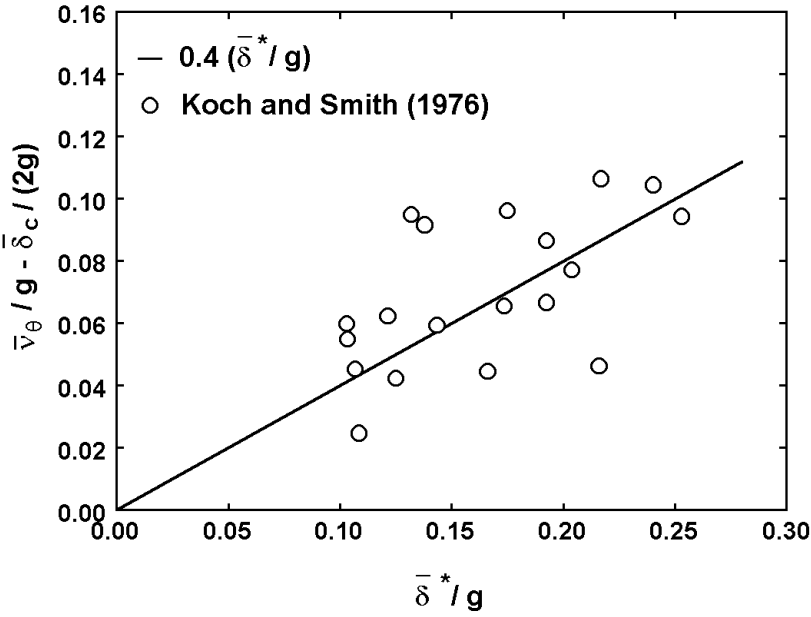

FIGURE 12-6 Tangential Force Defect Thickness

blade force defect thickness is modified by a term Δv to account for the influence of the blade guidance

$$v = v_0 + \Delta v \tag{12-45}$$

This correction term is computed exactly as was done in Chapter 8, using Eqs. (8-53) and (8-57), but with an alternate definition for the parameter, F, that is more suitable to integration within the blade passage. The form used for F is based on the following assumptions:

- The blades guide the flow toward collateral flow primarily close to the blade surfaces. It is assumed that the gap-averaged deviation from collateral flow imposed by integrating the boundary layer equations, using only v_0, will be reduced by about 50% due to the blade guidance.
- The influence of blade guidance and clearance gap on the blade force defect is negligible when the blade clearance gap is greater than the boundary layer thickness.
- The influence of blade guidance and clearance gap on the blade force defect is negligible at the blade row leading edge. This influence is assumed to be proportional to the ratio of the meridional distance to the blade spacing.

The second assumption simply recognizes the special case where the boundary layer and blades are not really interacting. Although this situation is probably very rare in a compressor, it can easily occur in the present analysis if the entrance boundary layer thickness is specified small enough. Experience has shown that this will lead to erratic and highly questionable results. The third assumption recognizes that the influence of the blades will not extend across the entire blade passage spacing until the flow penetrates well into the guided passage. This leads to the following approximation for F:

$$F = [1 - \delta_c / \delta]m / [(g + m] / 2 \; ; \delta_c \le \delta \tag{12-46}$$

$$F = 0; \delta_c > \delta \tag{12-47}$$

Equation (12-46) includes the influence of the ratio m/g, where m is the meridional distance from the blade leading edge and g is analogous to the local staggered spacing used in Chapter 8, i.e.,

$$g = 2\pi r \cos \beta' / Z \tag{12-48}$$

F is used directly in Eq. (8-57) and is also imposed as a correction applied to Eq. (12-44).

$$v_0 = 0.4\delta_1^* + \delta_c F \tag{12-49}$$

Since there are now several spatial integration steps within the blade passage, the blade force defect and the blade force direction given by Eq. (8-49) both vary

through the blade passage, but the process of numerical integration is the same as that used in Chapter 8. However, the calculation of Δv requires more care since it relates to a local blade force correction rather than an overall blade row correction. Locally, the ideal blade force may be extremely small, or even zero. This can produce unrealistic values of Δv. To avoid such problems, a constraint is imposed on Δv in the form

$$|\Delta v| \le [0.05 + 0.2(H_1 - 1)]\delta \tag{12-50}$$

This constrains the blade force correction to be less than about 75% of the meridional displacement thickness, except at values of H_1 very close to 1. The displacement thickness will vanish when $H_1 \to 1$, so special care is required to avoid suppressing the blade guidance effect entirely in that case.

Figures 12-7 and 12-8 show typical boundary layer parameters predicted by this end-wall boundary layer analysis when applied to the axial-flow compressor stator problem used as an example earlier in this chapter. This blade row operates at near optimum incidence angles at the operating conditions considered in this sample case. Hence, the blade row pressure coefficient is relatively mild for this case. Based on the experimental data shown in Fig. 8-2, the blade force defect thickness, averaged over the blade row, is expected to be a fairly large fraction of the meridional displacement thickness, which is at least consistent with

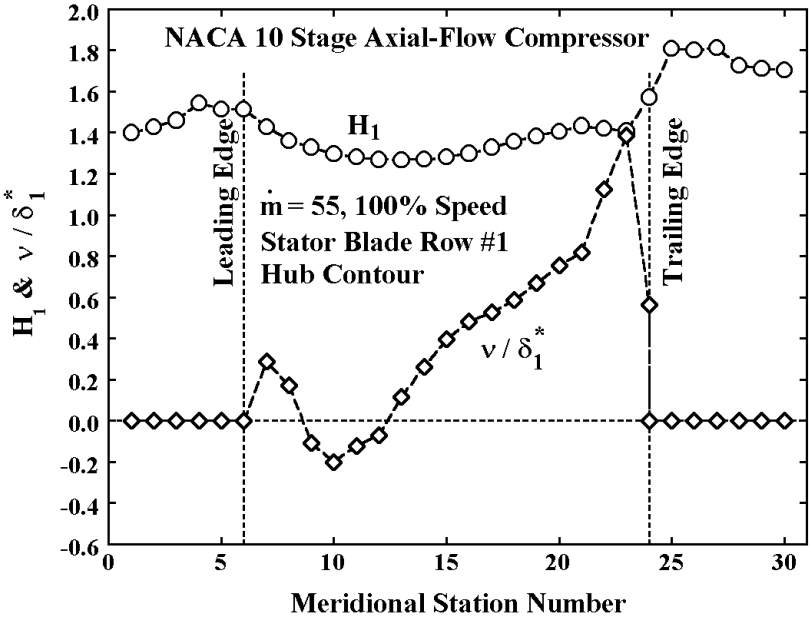

FIGURE 12-7 Hub Contour Boundary Layer

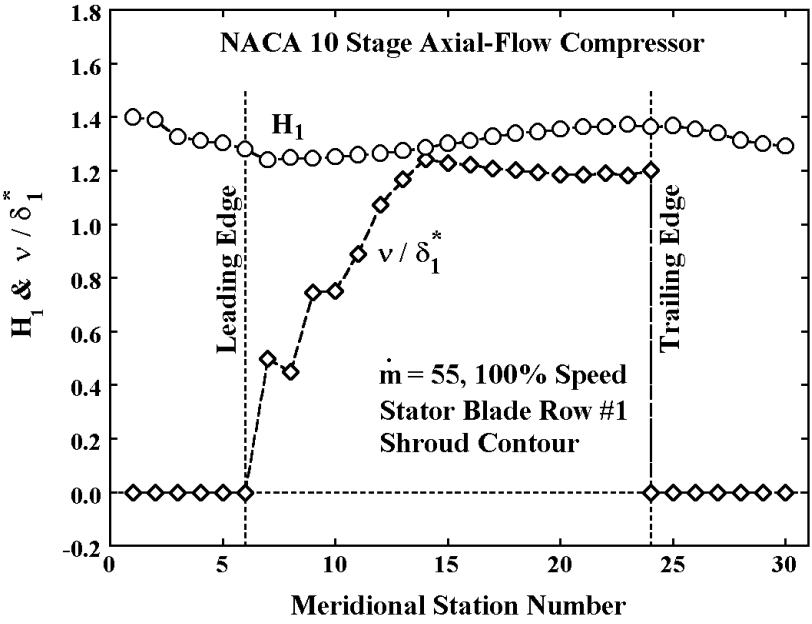

FIGURE 12-8 Shroud Contour Boundary Layer

the present predictions. That certainly does not provide a real validation of the assumptions, nor is there any data available in the literature suitable for validating them. The assumptions are considered reasonable, and they produce results consistent with overall blade row experimental data. Also, they produce no obvious deficiencies such as those seen from the simpler model of Aungier (2000). That is about all that can be said to justify their use.